NANS-mediated synthesis of sialic acid is required for brain and skeletal development

Clara D M van Karnebeek[1,2,28], Luisa Bonafé[3,28], Xiao-Yan Wen[4,5,28], Maja Tarailo-Graovac[2,6], Sara Balzano[7], Beryl Royer-Bertrand[3,7], Angel Ashikov[8], Livia Garavelli[9], Isabella Mammi[10], Licia Turolla[11], Catherine Breen[12], Dian Donnai[12], Valerie Cormier[13], Delphine Heron[13], Gen Nishimura[14], Shinichi Uchikawa[15], Belinda Campos-Xavier[3], Antonio Rossi[16], Thierry Hennet[17], Koroboshka Brand-Arzamendi[4,5], Jacob Rozmus[1], Keith Harshman[18], Brian J Stevenson[19], Enrico Girardi[20], Giulio Superti-Furga[20,21], Tammie Dewan[1], Alissa Collingridge[1], Jessie Halparin[1], Colin J Ross[1,2,6], Margot I Van Allen[6], Andrea Rossi[22], Udo F Engelke[23], Leo A J Kluijtmans[23], Ed van der Heeft[23], Herma Renkema[23], Arjan de Brouwer[24], Karin Huijben[23], Fokje Zijlstra[23], Thorben Heisse[25], Thomas Boltje[25], Wyeth W Wasserman[2,6], Carlo Rivolta[7], Sheila Unger[26], Dirk J Lefeber[8,23], Ron A Wevers[23,29] & Andrea Superti-Furga[3,27,29]

We identified biallelic mutations in *NANS*, the gene encoding the synthase for *N*-acetylneuraminic acid (NeuNAc; sialic acid), in nine individuals with infantile-onset severe developmental delay and skeletal dysplasia. Patient body fluids showed an elevation in *N*-acetyl-D-mannosamine levels, and patient-derived fibroblasts had reduced NANS activity and were unable to incorporate sialic acid precursors into sialylated glycoproteins. Knockdown of *nansa* in zebrafish embryos resulted in abnormal skeletal development, and exogenously added sialic acid partially rescued the skeletal phenotype. Thus, NANS-mediated synthesis of sialic acid is required for early brain development and skeletal growth. Normal sialylation of plasma proteins was observed in spite of NANS deficiency. Exploration of endogenous synthesis, nutritional absorption, and rescue pathways for sialic acid in different tissues and developmental phases is warranted to design therapeutic strategies to counteract NANS deficiency and to shed light on sialic acid metabolism and its implications for human nutrition.

Intellectual developmental disorders (IDDs) affect 2–2.5% of children and adults worldwide[1]. The developmental origin of IDDs is reflected in their definition as "substantial impairments of intellectual function and social or adaptive functioning present from early childhood" (ref. 2). Recent advances have shown that, in many cases, the etiology of these disorders is genetic, most frequently involving *de novo* mutations[3,4]. Along with a better understanding of the surrounding condition and prognosis, insights into the molecular basis of neurocognitive impairment allow for the development and application of targeted therapeutic strategies[5]. Although less frequent than IDDs, genetic disorders affecting skeletal development and growth (commonly called 'skeletal dysplasias') are a group of over 500 distinct disorders[6].

[1]Department of Pediatrics, University of British Columbia, Vancouver, British Columbia, Canada. [2]Centre for Molecular Medicine, Child and Family Research Institute, University of British Columbia, Vancouver, British Columbia, Canada. [3]Centre for Molecular Diseases, Lausanne University Hospital (CHUV), University of Lausanne, Lausanne, Switzerland. [4]Zebrafish Centre for Advanced Drug Discovery, Keenan Research Centre for Biomedical Science, St. Michael's Hospital, Toronto, Ontario, Canada. [5]Department of Medicine, University of Toronto, Toronto, Ontario, Canada. [6]Department of Medical Genetics, University of British Columbia, Vancouver, British Columbia, Canada. [7]Department of Medical Genetics, University of Lausanne, Lausanne, Switzerland. [8]Department of Neurology, Donders Institute for Brain, Cognition and Behavior, Radboud University Medical Center, Nijmegen, the Netherlands. [9]Clinical Genetics Unit, IRCCS-S. Maria Nuova Hospital, Reggio Emilia, Italy. [10]Ambulatorio di Genetica Medica ULSS 13, U.O. Ginecologia e Ostetricia, Ospedale Dolo, Dolo, Italy. [11]Medical Genetics Unit, Local Health Authority (ULSS 9), Treviso, Italy. [12]Manchester Centre for Genomic Medicine, Institute of Human Development, Faculty of Medical and Human Sciences, University of Manchester, St. Mary's Hospital, Central Manchester University Hospitals NHS Foundation Trust, Manchester Academic Health Science Centre, Manchester, UK. [13]Institut IMAGINE, Hôpital Necker–Enfants Malades, Paris, France. [14]Department of Radiology, Tokyo Metropolitan Children's Medical Center, Tokyo, Japan. [15]Department of Orthopedics, National Center for Child Health and Development, Tokyo, Japan. [16]Department of Molecular Medicine, Unit of Biochemistry, University of Pavia, Pavia, Italy. [17]Department of Physiology, University of Zürich, Zurich, Switzerland. [18]Genomic Technologies Facility, Faculty of Biology and Medicine, University of Lausanne, Lausanne, Switzerland. [19]Vital-IT Group, Swiss Institute of Bioinformatics, University of Lausanne, Lausanne, Switzerland. [20]CeMM Research Center for Molecular Medicine of the Austrian Academy of Sciences, Vienna, Austria. [21]Center for Physiology and Pharmacology, Medical University of Vienna, Vienna, Austria. [22]Neuroradiology Department, G. Gaslini Children's Hospital, Genoa, Italy. [23]Translational Metabolic Laboratory, Department of Laboratory Medicine, Radboud University Medical Center, Nijmegen, the Netherlands. [24]Department of Genetics, Radboud University Medical Center, Nijmegen, the Netherlands. [25]Department of Organic Chemistry, Radboud University, Nijmegen, the Netherlands. [26]Medical Genetics Service, Lausanne University Hospital, University of Lausanne, Lausanne, Switzerland. [27]Department of Pediatrics, Lausanne University Hospital, University of Lausanne, Lausanne, Switzerland. [28]These authors contributed equally to this work. [29]These authors jointly supervised this work. Correspondence should be addressed to A.S.-F. (asuperti@unil.ch), R.A.W. (ron.wevers@radboudumc.nl) or C.D.M.v.K. (cvankarnebeek@cw.bc.ca).

Received 2 March; accepted 29 April; published online 23 May 2016; doi:10.1038/ng.3578

Studying their molecular basis has provided valuable insights into the many factors necessary for skeletal development, ranging from minerals and structural molecules to enzymes and to signaling molecules and transcription factors[6,7]. We report here a genetic disorder presenting as a combination of severe IDD with skeletal dysplasia and short stature. Our data show that the pathogenic basis of this disorder is an inborn error of metabolism that affects the endogenous synthesis of NeuNAc. Exploration of the biochemical and molecular features of this disorder provides new information on the role of sialic acid in the development of brain and bone.

RESULTS

Clinical and radiographic phenotypes of NANS deficiency

Clinical patient reports are presented *in extenso* in the **Supplementary Note**. Nine patients from six families were studied; patients 1, 2, and 5 have previously been described[8,9]. The main clinical features of the disorder included a prenatal history that was unremarkable in all patients except for one (patient 8), in whom prenatal hydrocephalus was diagnosed. No specific signs and symptoms were present at birth, except for disproportionately short limbs that were observed in three patients (patients 3, 8, and 9). In the first months of life, all patients showed muscle hypotonia, and the achievement of early developmental milestones such as sitting and walking was delayed. Subsequently, global developmental delay, including cognitive impairment, was the major medical concern. All adult patients showed moderate-to-severe IDD; only one patient acquired speech, and none was living independently. Seizures were a prominent and early feature in one patient but were infrequent in some and absent in others. Social competences were relatively preserved. Body measurements at birth were normal or slightly lower than normal, but growth velocity decreased during the first or second year of life, and short stature with shortening of both the trunk and limbs was present in all adult patients. Facial features included a prominent forehead, mild synophrys, a sunken nasal bridge, a prominent bulbous nasal tip, and full lips (**Fig. 1**). No endocrine anomalies were noted, and adult patients had gone through pubertal development. Neuroimaging was available for six patients: patient 8 showed prenatal-onset hydrocephalus, whereas patient 9 showed perisylvian polymicrogyria, small basal ganglia, and reduced white matter mass (**Supplementary Fig. 1**); the other four patients showed moderate cerebral atrophy with nonspecific changes in white matter. Distinct features that permitted these individuals to be distinguished from among the large group of persons with severe IDD included the facial dysmorphisms and the skeletal dysplasia with short stature, premature carpal ossification, platyspondyly, longitudinal metaphyseal striations, and small epiphyses (see **Fig. 1** for details). For more radiographic details, see also the previous clinical reports for patients 1 and 2 (ref. 8) and for patient 5 (corresponding to patient 1 in ref. 9).

Identification of *NANS* mutations and functional analysis

Exome sequencing was performed on genomic DNA from patients 1–4. After passage through the filtering pipeline (Online Methods and **Supplementary Table 1**), only one gene, *NANS*, showed biallelic variants in all four patients (**Table 1**). A small indel just 5′ to exon 4, c.449–10_449–5delGATTACinsATGG, was seen in a heterozygous state in all four patients (reference transcript ENST00000210444, NCBI reference sequence NM_018946.3). In addition to this shared mutation, patients 1 and 2 (who are sisters) had a single-nucleotide insertion predicted to result in a frameshift with early truncation (c.389_390insT, p.Lys131Glnfs*8), whereas patients 3 and 4 (who are brother and sister) had a mutation of a canonical splice donor site (c.448+1G>A). Computational haplotype reconstruction using exome data identified a specific haplotype encompassing a region of 1.38 Mb on chromosome 9 (from 100,388,119 (rs10817858) to 101,767,385 (rs41305481) bp) in the four individuals carrying the intronic indel, indicative of a common origin for this variant. Sanger sequencing was used to confirm the mutations and to verify segregation with disease in all families. To test for the pathogenicity of the identified variants, *NANS* cDNA was retrotranscribed from fibroblast or lymphoblastoid cell RNA from patients 1, 3, and 4, as well as from the parents of patients 3 and 4, incubated with or without cycloheximide, PCR amplified, and analyzed by capillary electrophoresis (**Supplementary Fig. 2**). The c.449–10_449–5delGATTACinsATGG indel (patients 1–4) resulted in very low levels of mRNA, with the presence of wild-type mRNA as well as an isoform lacking both exons 3 and 4 (in frame); in the presence of cycloheximide, this allele seemed to produce additional abnormal isoforms, which apparently were subject to nonsense-mediated RNA decay (NMD). The c.448+1G>A variant (patients 3 and 4) produced two splicing isoforms, one lacking both exons 3 and 4 (similar to the previous mutation) and expressed at levels comparable to the wild-type allele and an out-of-frame isoform lacking exon 3 and part of exon 4 that was detected at very low levels. The exonic insertion c.389_390insT (patients 1 and 2) triggered NMD, as demonstrated by sequencing RT–PCR clones obtained from cells with or without cycloheximide treatment. Thus, all three mutations resulted either in unstable or nonfunctional *NANS* mRNA or in reduced levels of wild-type transcripts. We then screened patients 5–8 by selective PCR amplification of *NANS* exons from genomic DNA and direct bidirectional Sanger sequencing of the amplicons and found biallelic mutations in all the patients, including four missense mutations and one triplet insertion leading to the duplication of one amino acid (**Fig. 2** and **Table 1**).

Investigation of patient 9, the youngest patient in our series, followed a different course; this patient was enrolled into the TIDEX study, which combines genomics and metabolomics screening[10]. Metabolomic screening had identified an unusual metabolite, *N*-acetyl-D-mannosamine (ManNAc), in the plasma and urine of this child. Among the variants identified by exome sequencing in this patient, two missense mutations in *NANS* stood out as ManNAc-6-phosphate is the substrate of the NANS enzyme and malfunction of this enzyme could account for the accumulation of ManNAc in body fluids. The *NANS* variants identified in patient 9 were confirmed via Sanger sequencing and were shown to segregate correctly in the family. Of note, the exome results for patients 1–5 were examined for possible pathogenic mutations in the *GNE* gene, but none were observed. After this stage, the data from patients 1–8 and those from patient 9 were combined for all subsequent studies.

Mapping of mutations on the three-dimensional protein model of NANS

The NANS protein was modeled as a homodimer on the basis of the *Neisseria meningitidis* homolog, as well as recent results supporting dimer formation for the human protein[11]. Of the predicted amino acid changes (**Table 1**), four mapped in or near the active site: p.Lys131Gln, p.Gly133Val, p.Tyr188His, and p.Pro189Leu. It is likely that any of these would affect the catalytic activity of the enzyme, by changing the ability of the protein to bind substrate (Lys131 and Tyr188 are also predicted to make hydrogen bonds with substrates[11]; **Fig. 2**), by changing the pocket shape (p.Gly133Val), or by affecting functional residues in the active site (Pro189 is located right next to Tyr188). The p.His29Asn and p.Arg237Cys substitutions are localized at the dimer interface and likely affect protein folding, stability, and/or dimer formation. Although close to the dimer interface, the Ile327 residue that is duplicated is not involved in protein contacts in our model, the

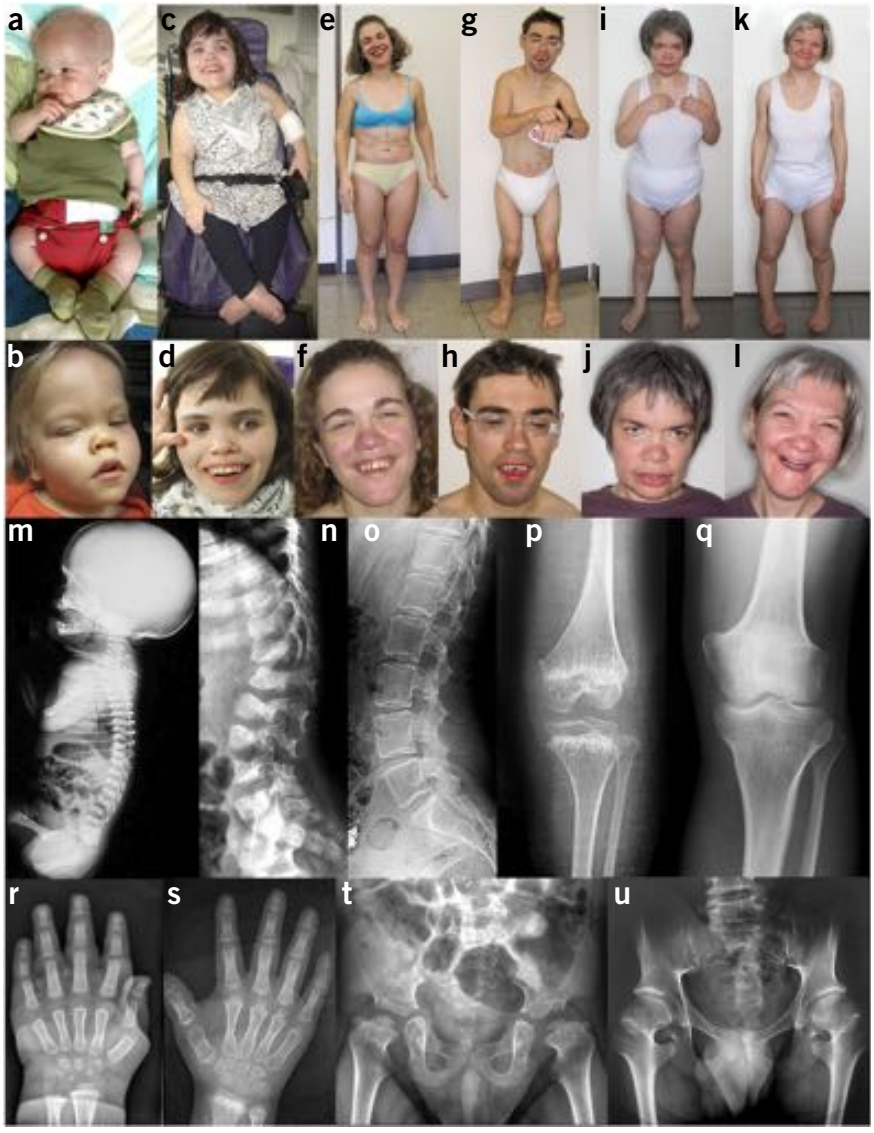

Figure 1 Morphological and skeletal features of NANS-deficient patients. (**a**,**b**) Patient 9 at age 6 months (**a**) and at age 3 years (**b**). (**c**,**d**) Patient 8 at age 28 years. (**e**,**f**) Patient 4 at age 24 years. (**g**,**h**) Patient 3 at age 28 years. (**i**,**j**) Patient 2 at age 38 years. (**k**,**l**) Patient 1 at age 40 years. For patient 9, only the phenotype of short limbs is apparent at age 6 months; facial dysmorphism with prominent forehead, saddle nose, full lips, and coarsening of traits is apparent at age 3 years. All adult patients have short stature (height between 130 and 150 cm). All photographs were obtained and published with consent. (**m**–**o**) Lateral spine films showing coronal clefts at birth (patient 8) (**m**) and severe vertebral body dysplasia at age 3 years (patient 9) (**n**); in adulthood, the vertebral bodies have a normal shape (patient 2) (**o**). (**p**,**q**) At the knees, there are metaphyseal striations and small epiphyses (epimetaphyseal dysplasia) at age 9 years (patient 8) (**p**); in adulthood, epiphyses remain small, whereas metaphyseal striations have disappeared (patient 2) (**q**). (**r**,**s**) Advanced carpal ossification at age 21 months (patient 9) (**r**) and metaphyseal striations (distal radius) with epiphyseal dysplasia at age 9 years (patient 8) (**s**). (**t**,**u**) Short femoral necks and small, irregular capital femoral epiphyses (epimetaphyseal dysplasia) at age 3 years, 7 months (patient 9) (**t**); in the adult (patient 3), short femoral neck and small epiphyses are present, but bone and cartilage structure appear normal (**u**). Compare the radiographic images of patients 1 and 2 and patient 5, as reported earlier[8,9].

duplication could be affecting folding instead. Finally, p.Arg151His is located on the surface of the protein and away from the dimer interface and substrate-binding site, possibly interfering with folding or with a critical protein interaction.

NANS mutations lead to accumulation of *N*-acetylmannosamine *in vivo*

Next-generation metabolic screening (Online Methods) was first applied to the cerebrospinal fluid (CSF) of patient 9 (**Fig. 3** and **Supplementary Table 2**) and then to the plasma of patients 1–4 and 9 (data not shown), leading to the identification of an unusual compound, ManNAc, in all five patients. Quantitative nuclear magnetic resonance (NMR) spectroscopy was then used to determine the concentration of ManNAc in available urine samples from patients. In patients 1–4 and 8 (all adults at the time of study), the urine concentration of ManNAc ranged from 41 to 98 µmol/mmol creatinine (reference values, <10 µmol/mmol creatinine), whereas the excretion of ManNAc was highest (295 µmol/mmol creatinine) in patient 9 (age 3 years). NMR spectroscopy was applied to homogenates of cultured fibroblasts to explore the intracellular sialic acid synthesis pathway. In fibroblasts from two unrelated patients (patients 3 and 9), this analysis showed increased intracellular levels of ManNAc-6-phosphate rather than free ManNAc in comparison to control cells. NANS can act as a NeuNAc phosphate synthase (MIM 605202; Enzyme Commission (EC) database 2.5.1.57). This may account for the accumulation of ManNAc in body fluids and ManNAc-6-phosphate within cells in patients. The free NeuNAc concentration in patient-derived fibroblasts was normal (**Supplementary Table 2**). Finally, we evaluated whether deficient NANS activity would lead to systemic deficiency for sialic acid. The concentration of free NeuNAc was evaluated in the urine of five patients from four families (relative to creatinine excretion) as well as in the CSF of patient 9. In all patients, normal values were found (**Supplementary Table 3**), suggesting that there was no systemic depletion of free neuraminic acid. Analysis of plasma transferrin and apolipoprotein C-III isoforms, to evaluate the biosynthesis of N- and O-linked glycans, respectively, has been carried out repeatedly on several of the patients in the clinical setting, with these analyses giving normal results (**Supplementary Table 4**). This evidence further contributes to the notion that peripheral sialylation is not significantly affected, despite NANS deficiency.

NANS mutations impair enzyme activity

In two preliminary experiments, we explored the sialylation of proteins and lipids at the cell surface of patient-derived and control fibroblasts using FITC-labeled *Sambucus nigra* lectin (which specifically binds to terminal galactose-bound sialic acid residues) and FACS analysis to determine the cellular content of CMP-NeuNAc

Table 1 Overview of the *NANS* mutations observed in the nine patients

Genomic DNA position on chr. 9 (bp)	cDNA change[a]	Exon	Protein change	Present in databases[b]	PolyPhen score	Provean score	Observed in patient(s)
100,819,175	c.85C>A	1	p.His29Asn	No	Probably damaging	Deleterious	Pt. 8
100,839,236	c.389_390insT	3	p.Lys131GlnfsTer8	WellderIy (0.0008)	NA	NA	Pts. 1 and 2
100,839,249	c.398G>T	3	p.Gly133Val	No	Probably damaging	Deleterious	Pts. 6 and 7
100,839,300	c.448+1G>A	3	Aberrant splicing of exons 3 and 4 as seen in mRNA studies	ExAC (0.00002633)	NA	NA	Pts. 3 and 4
100,840,462	c.449–10_449–5delGATTACinsATGG[c]	4	Aberrant splicing of exons 3 and 4 as seen in mRNA studies	ExAC (0.00004947)	NA	NA	Pts. 1 and 2 Pts. 3 and 4
100,840,478	c.452G>A	4	p.Arg151His	WellderIy (0.0008)	Probably damaging	Neutral	Pt. 5 (homozygous)
100,840,588	c.562T>C	4	p.Tyr188His	No	Probably damaging	Deleterious	Pt. 9
100,840,592	c.566C>T	4	p.Pro189Leu	No	Probably damaging	Deleterious	Pt. 8
100,843,203	c.709C>T		p.Arg237Cys	No	Probably damaging	Deleterious	Pt. 9
100,845,238	c.981insATC	6	p.Ile327dup	No	Probably damaging	Deleterious	Pts. 6 and 7

NA, not applicable.[a]Based on transcript ENST00000210444 (CCDS6733), NCBI reference sequence NM_018946.3. [b]The databases considered included the ExAC database (accessed November 2015) and the WellderIy database (accessed January 2016) (see URLs). [c]This mutation was flagged as the following two distinct events, both in our pipeline and in the ExAC browser: (i) an intronic insertion, chr. 9: g.100840462C>CTGA (http://exac.broadinstitute.org/variant/9-100840462-C-CTGA), and (ii) an intronic deletion, chr. 9: g.100840465GATTAC>G (http://exac.broadinstitute.org/variant/9-100840465-GATTAC-G). This is due to the fact that both our pipeline and the ExAC pipeline used GATK variant calling software (see URLs). In ExAC data, the 'two' mutational events have been seen in the same number of individuals of European origin. Sanger sequencing in our samples confirms that the variant is a single mutational event.

and total NeuNAc before and after the addition of 10 mM ManNAc[12]. No differences between patient-derived and control fibroblasts were seen, possibly because the concentration of ManNAc used was substantially higher than what is found physiologically. We then developed a method to measure NANS enzyme activity in cell lysates by incubating lysates with ManNAc-6-phosphate and phosphoenolpyruvate (PEP) and quantifying newly formed NeuNAc by mass spectrometry (**Fig. 3d**). In comparison with fibroblasts from five healthy controls (613 ± 150 nmol NeuNAc/mg protein, mean ± s.d.), the three available patient-derived fibroblast lines showed reduced production of NeuNAc (163 ± 111 nmol NeuNAc/mg protein, mean ± s.d.) after 24 h of incubation. Fibroblasts from the heterozygous father of patients 3 and 4 showed intermediate NANS activity (403 nmol NeuNAc/mg protein). Although residual activity in this assay was high, these results are in agreement with an autosomal recessive defect in *NANS*.

Incorporation of *N*-acetyl-D-mannose into sialoglycoproteins is impaired

We then applied metabolic labeling of sialic acids using propargyloxycarbonyl (Poc)-derivatized analogs of ManNAc and NeuNAc (ManNPoc and NeuNPoc, respectively)[13], in a recently developed technique that had been useful in confirming deficient sialic acid incorporation in cells deficient for the Golgi transporter of CMP–sialic acid[14]. NeuNPoc, which enters the metabolic pathway downstream of the enzymatic step catalyzed by NANS, was incorporated efficiently into glycoproteins in all cell lines analyzed, whereas ManNPoc, which enters the pathway upstream of the NANS-catalyzed step (**Fig. 4**), was incorporated in fibroblasts from a control and a heterozygote for a *NANS* mutation but not in fibroblasts from patients 3, 8, and 9 (**Fig. 3e**). These data confirm the functional impairment of NANS activity in the metabolic pathway of sialic acid biosynthesis and protein sialylation. NANS deficiency should therefore be included on the list of congenital disorders of glycosylation (CDGs). Notably, these data suggest that exogenous NeuNAc might be used to bypass the enzymatic block.

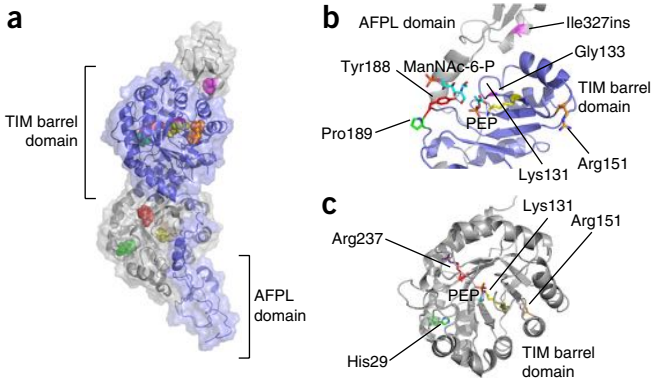

Figure 2 Three-dimensional model of the NANS protein and mapping of amino acid residues affected by mutations. (**a**) Model of the human NANS protein, showing one monomer in gray and one monomer in blue. Mutated residues are color-coded according to patient, with each allele mapped on a separate monomer. Lys131 and Arg151 are shown on both monomers. (**b**,**c**) Detailed views of the location of the alterations. PEP, phosphoenolpyruvate; TIM, triose phosphate isomerase.

nansa knockdown perturbs zebrafish skeletal development

There are two zebrafish orthologs for the human *NANS* gene, the *nansa* and *nansb* genes (see the Online Methods for details). *nansa* is expressed during early embryonic development, including during the stages with 50% epiboly in the axis, 1–13 somites at the notochord and polster, and 14–19 somites at the hatching gland. Thereafter, *nansa* is strongly expressed in the head, immature eye, myotome, optic tectum, and pharyngeal arch skeleton[15]. The expression pattern of *nansb* is unknown. We designed morpholino oligonucleotides (MOs) that block splicing to knock down both the *nansa* and *nansb* genes[16] (Online Methods). Microinjection of *nansa* MO into newly fertilized zebrafish eggs resulted in embryos with a small head, pericardial edema, and developmental anomalies of the skeleton, highlighted by Alcian blue staining, at 6 days post-fertilization (d.p.f.) (**Fig. 5a**,**b**). Interestingly, *nansa* morphants showed a complex phenotype in the area of the head, including hypoplastic or absent Meckel's cartilage, a lack of basihyal, shortened and abnormal ethmoid plate, trabecula, parachordal and palatoquadrate, and absence of the ceratobranchial structures (**Fig. 5b**)[17]. *nansb* morphants did not show an overt abnormal phenotype even at higher concentrations of the MOs (data not shown).

Partial rescue of skeletal development by exogenous NeuNAc

Given the position of Nansa (and NANS in human) in the synthetic pathway of NeuNAc, we tested whether the addition of sialic acid in zebrafish embryo water would rescue the head and skeleton

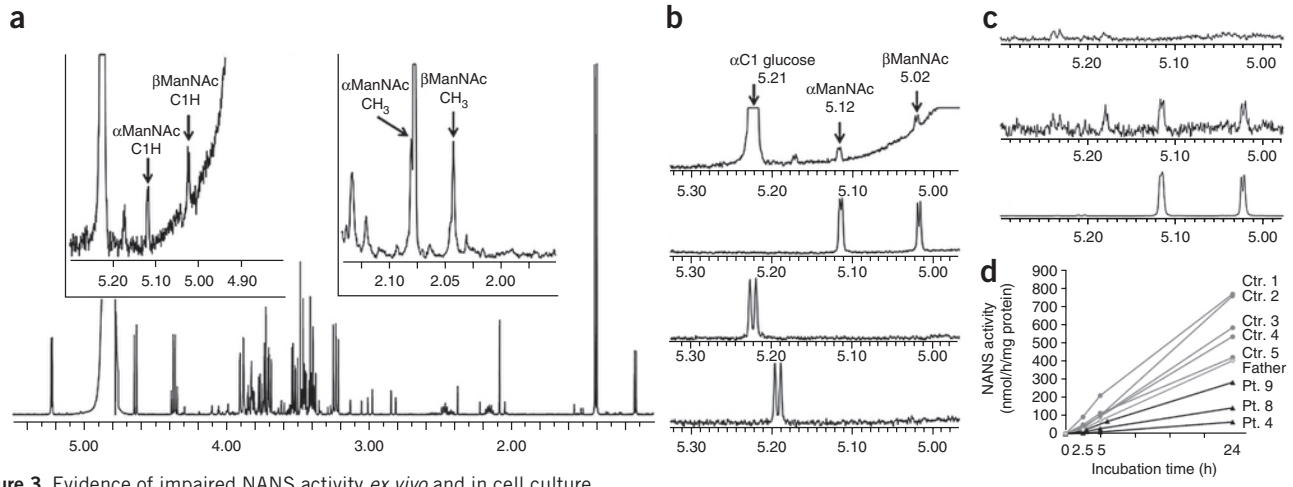

Figure 3 Evidence of impaired NANS activity *ex vivo* and in cell culture. (**a**–**c**) 500-MHz one-dimensional ^{1}H NMR spectra of body fluids and model compounds (the horizontal axis shows the chemical shift; the vertical axis reflects the relative intensity of a metabolite). (**a**) CSF from patient 9 contains ManNAc at a concentration of 180 μM (reference, <5 μM). "αManNAc C1H" represents resonance from the proton on carbon atom number 1 in the alpha anomeric form of *N*-acetylmannosamine; "αManNAc CH3" represents resonance from protons in the methyl group in the *N*-acetyl part of *N*-acetylmannosamine). Resonances of alpha and beta forms of *N*-acetylmannosamine are shown in the insets. (**b**) Top to bottom, resonances of the alpha and beta forms of ManNAc for the inset-relevant part of the CSF spectrum in **a** in comparison to the spectra for ManNAc, GalNAc (*N*-acetylgalactosamine), and GlcNAc (*N*-acetylglucosamine). (**c**) Top to bottom, spectra obtained from the fibroblasts of a control and patient 8 and the spectrum for a model compound, ManNAc-6-phosphate. (**d**) NANS enzyme activity in fibroblast lysates. Fibroblast lysates were from five controls (Ctr.), the heterozygous father of patients 3 and 4 (Father), and patients 4, 8, and 9. For details on the enzyme assay, see the Online Methods. (**e**) Metabolic labeling of sialylated proteins. Fibroblasts from a control, the heterozygous father of patients 3 and 4, and patients 4, 8, and 9 (**Table 1**) were incubated with peracetylated propargyloxycarbonyl analogs of ManNAc and NeuNAc—ManNPoc and NeuNPoc, respectively (see **Fig. 4** for the entry point of these molecules in the sialic acid biosynthetic pathway). Cell proteins were detected by immunoblotting using streptavidin-HRP (top) or antibody against GAPDH (bottom) as an internal control. In cells from the control and the heterozygous father, both ManNPoc and NeuNPoc result in strong labeling of proteins. In patient-derived cells, ManNPoc (which enters the synthetic pathway upstream of NANS) is unable to label proteins, whereas NeuNPoc (which enters the pathway downstream of the NANS enzyme) is incorporated efficiently. These findings confirm a metabolic block between ManNAc and NeuNAc, consistent with impaired NANS activity.

developmental phenotypes of *nansa* morphants. Addition of sialic acid at a concentration of 200 μM resulted in partial rescue of the skeletal phenotype, as measured by the reappearance and development of Meckel's cartilage structure; this structure was correctly formed in 9% of embryos under baseline *nansa* knockdown conditions but in 61% of embryos when sialic acid was added to the water (**Fig. 5c**,**d**).

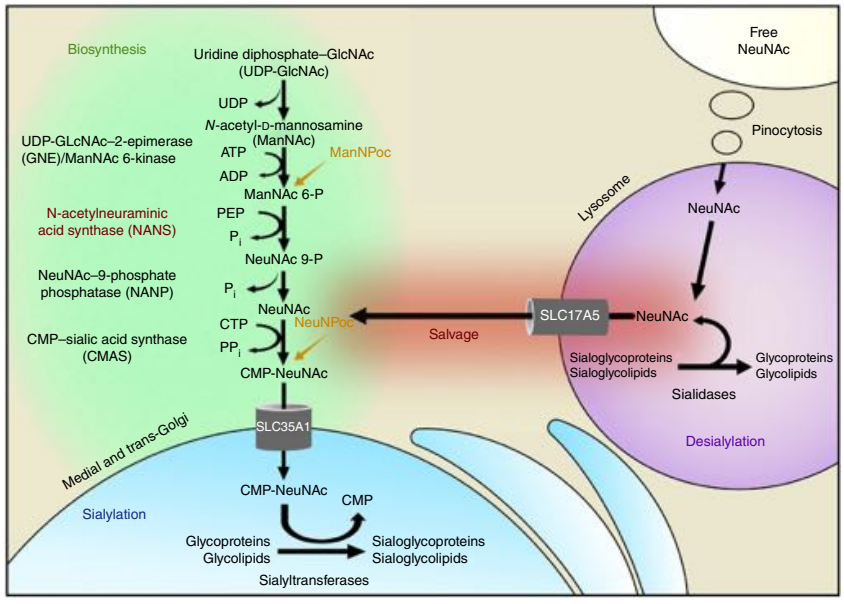

Figure 4 Simplified scheme of *N*-acetylneuraminic acid metabolism in human. Biosynthesis of NeuNAc is achieved largely in the cytoplasm, except for the CMP–sialic acid synthase (CMAS) reaction, which takes place in the nucleus (the nuclear envelope and its possible transporters are omitted here for simplicity). The synthesis of ManNAc is carried out in two steps by the bifunctional enzyme GNE/ManNAc 6-kinase. NeuNAc synthase (NANS) is highlighted in red. CMP–sialic acid is transferred by a specific transporter, SLC35A1, into the medial and trans-Golgi apparatus, where it is used as a substrate for the sialylation of proteins and lipids by various sialyltransferases. When sialylated glycoproteins and lipids are degraded in the lysosome, the free sialic acid released by sialidases can diffuse out of the lysosome through the lysosomal sialic acid transporter (SLC17A5). Free NeuNAc (as well as non-human sialic acid, NeuNGc) can be taken up by pinocytosis and released into the cytoplasm by the SLC17A5 transporter. Free sialic acid can then reenter the biosynthesis pathway (indicated as 'salvage' in the scheme). The relative importance of biosynthesis and salvage in different cell types and tissues is largely unknown. The metabolic scheme also shows the entry points of the two synthetic analogs used in this study, ManPoc and NeuNPoc, with the first being upstream and the second downstream of the step catalyzed by NANS.

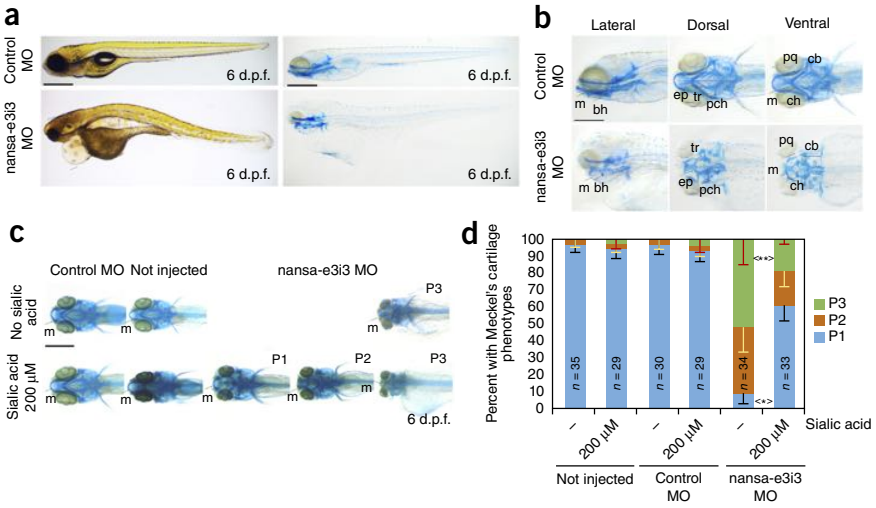

Figure 5 Abnormal skeletal development in zebrafish with morpholino-mediated knockdown of *nansa* is partially rescued by exogenous sialic acid. (**a**,**b**) nansa-e3i3 morphants (4 ng/nl) display a small head, pericardial edema, and abnormal cartilage and skeleton development, including hypoplastic or absent Meckel's cartilage (m) and lack of basihyal (bh) together with shortened and abnormal ethmoid plate (ep), trabecula (tr), parachordal (pch), palatoquadrate (pq), and ceratobranchial (cb) structures (dorsal and ventral views). ch, ceratohyal cartilage. Scale bars, 500 µm in **a** and 200 µm in **b**. (**c**) 200 µM sialic acid partially rescues the abnormal skeletal phenotype, as assessed by Meckel's cartilage measurement: P1, complete Meckel's cartilage; P2, incomplete Meckel's cartilage; P3, absent Meckel's cartilage. Scale bar, 200 µm. (**d**) The graph shows the proportion of fish with a Meckel's cartilage phenotype of P1, P2, or P3 with or without exogenously added sialic acid. For each experimental condition, approximately 10–12 embryos were analyzed (exact numbers are shown in the figure); experiments were carried out in triplicate. Error bars, s.d. from triplicate experiments. For *nansa* morphants, the difference between embryos with and without 200 µM sialic acid is statistically significant: $*P = 0.05$ for P1 embryos, $**P = 0.01$ for P3 embryos (two-tailed *t* test).

Interestingly, the rescue effect of sialic acid was dependent on the timing of its addition; rescue was observed when sialic acid was added to the embryo water right after MO injection but not when it was added 24 hours post-fertilization (h.p.f.), suggesting that sialic acid has a critical role in early embryonic development, potentially in cartilage and skeleton cell lineage specification or growth.

DISCUSSION

We present evidence that biallelic deleterious mutations in *NANS* are associated with severe IDD and skeletal dysplasia. First, we identified ten different *NANS* variants in nine patients from six unrelated families, segregating according to a recessive disease model. Second, the *NANS* mutations impaired the activity of the NeuNAc synthase enzyme, as evidenced by reduced enzyme activity and by the specific block of ManNAc analog incorporation in cultured cells. Third, dysfunction of NANS *in vivo* was confirmed by the accumulation of substrates of the missing enzyme, ManNAc in body fluids and ManNAc-6-phosphate in cultured cells. Finally, inactivation of the enzyme activity in zebrafish embryos resulted in a complex phenotype including abnormal development of skeletal structures. The conclusion that *NANS* mutations are the cause of the clinical phenotype is strengthened by the fact that it was reached by two independent approaches. Patients 1–8 were ascertained because of their phenotype of intellectual disability and specific skeletal dysplasia, and the genomic approach led to identification of *NANS* mutations and to their validation through RNA studies. Patient 9 was subjected to metabolomic screening first to elucidate the cause of severe IDD and dysmorphisms, leading to the identification of ManNAc in body fluids, and this biochemical phenotype allowed us to prioritize *NANS* mutations as the most likely to be pathogenic among the variants found subsequently through exome sequencing. Although most of our patients were ascertained retrospectively and the clinical assessment is heterogeneous, there are indications of different degrees of clinical severity. The study of additional patients is needed to determine the clinical spectrum of NANS deficiency and to establish possible genotype–phenotype correlations.

The brain contains the highest concentration of total sialic acid among human organs[18]. Sialic acid is present on glycoproteins and glycolipids such as the gangliosides, which are particularly abundant in nervous tissue, and NANS is highly expressed in the human brain (**Supplementary Fig. 3**). Genetic deficiency of either the sialyltransferase ST3GAL3 (MIM 604402) or ST3GAL5 (MIM 609056), two enzymes that use CMP-NeuNAc to add terminal sialic acid residues to the glycosidic antennae of glycoproteins and glycolipids, leads to infantile epilepsy and/or developmental arrest, suggesting that appropriately sialylated glycoproteins and/or glycolipids are necessary for higher brain functions[19–22]. Mutations affecting the CMP-NeuNAc transporter SLC35A1 (MIM 605634; see **Fig. 4**) result in developmental disability with ataxia and bleeding diathesis[23]. The observation of IDD in NANS-deficient patients and the brain dysplasia observed in two of them underline the relationship between sialylation and neurological functions and suggest that the requirements for sialic acid in the developing brain must be met at least partially by endogenous synthesis of sialic acid through the NANS pathway.

The short stature and skeletal dysplasia in NANS-deficient individuals also indicate that NANS-mediated sialic acid synthesis has a pivotal role in skeletal development, specifically in growth plate cartilage. The skeletal anomalies seen in the zebrafish knockdown model support this notion. The avascular nature of cartilage may make it dependent on endogenous synthesis. Several of the key players in cartilage and bone growth and development, such as chondroitin sulfate proteoglycans[24], bone sialoprotein[25], and osteopontin[26], are heavily sialylated and are candidates for further studies.

Tests detecting hyposialylated transferrin and apolipoprotein C-III yielded normal results in our NANS-deficient patients, and there was no clinical or laboratory evidence of hyposialylation of plasma proteins or clotting factors, suggesting that sialylation of plasma proteins is not greatly affected. How sialylation is achieved with impaired NANS activity is unclear. Several lines of explanation can be considered. First, the mutations in our patients may allow for some residual activity; none of our patients had a combination of two bona fide null alleles. Second, endogenous NeuNAc synthesis may be rate limiting in certain tissues and at certain times, where and when synthetic requirements are maximal (such as in the brain, during periods of rapid growth before birth and in the first 2 years of life[27–29], or in cartilage during infancy and childhood) but not in other tissues where

synthetic requirements for sialic acid may be lower. Such a mechanism has been put forward to explain the muscle-restricted phenotype of GNE myopathy (MIM 603824)[30], a disorder caused by recessive mutations in the *GNE* gene encoding UDP-*N*-acetylglucosamine 2-epimerase and ManNAc kinase activities in the sialic acid synthesis pathway (**Fig. 4**). Third, some tissues may be able to rescue and recycle sialic acid derived from the lysosomal breakdown of sialylated macromolecules (**Fig. 4**). A fourth possibility, not mutually exclusive with the others, is that nutrition-derived sialic acids may be entered into biosynthetic pathways and that this may occur in some tissues, such as the liver, but not or to a lesser extent in brain or cartilage. The observation of normal levels of free sialic acid in the urine of our NANS-deficient patients also indicates that there is no systemic depletion of sialic acid.

The role of nutrition-derived sialic acid raises the question of a possible treatment with oral sialic acid in NANS-deficient individuals, in analogy to other glycosylation and sialylation defects, such as CDG1B (MIM 602579) and GNE myopathy[31], which have been amenable to treatment by oral administration of specific sugars. Some of our data may point in this direction. When added to patient-derived cells in culture, the sialic acid analog NeuNPoc (used because of its detectability) but not the upstream metabolite ManNPoc was able to bypass the enzymatic block and be incorporated into macromolecules. In zebrafish embryos, exogenously added sialic acid was able to partially recue the developmental phenotype caused by *nansa* knockdown. It is possible that dietary supplementation with sialic acid could be beneficial for NANS-deficient patients. There is evidence that free sialic acid can be taken up and metabolized by cultured cells[32]; this could occur through pinocytosis and release to the cytoplasm by the lysosomal sialic acid exporter (SLC17A5; **Fig. 4**). In young mice and rats, sialic acid injected in the peritoneum is incorporated into macromolecules[33], and orally administered free sialic acid is found in plasma and, subsequently, in the liver and the brain[29,33]. *N*-glycolylneuraminic acid, a sialic acid analog that is widespread in mammals and apes but absent in man because of an evolutionary mutation, is found in human tissues as the result of dietary uptake from meat products[34,35]. Altogether, there is evidence suggesting that alimentary sialic acids could potentially be taken up and incorporated into biosynthetic pathways in human. The relative contributions of endogenously synthesized, nutritionally derived, and rescued sialic acid in different tissues and at different developmental stages in man remain to be investigated and may explain how the consequences of NANS deficiency are restricted to the developing brain and cartilage. In particular, if the brain pathology in NANS deficiency occurs in the first months of life (and perhaps even prenatally), this might be an obstacle to efficient treatment. Extensive studies in cell culture and *in vivo* are needed before envisaging any treatment possibility for NANS-deficient individuals. Such studies would also have the potential of clarifying the role of nutritional sialic acid in human.

Human milk contains a high concentration of free oligosaccharides, most of which are sialylated[27,28,36,37], as well as free sialic acid. These oligosaccharides, which are notably absent from cow's milk and infant formulas, have been attributed numerous functions, including stimulating brain development and cognition in infants[27,28,37,38]. Because oral administration of sialic acid in humans is considered safe and is well tolerated, nutritional supplementation with sialic acid in infancy, gestation, and advanced age has been proposed[27–29,37]. In view of the role of sialic acid and its potential use in nutrition, exploring the pathogenesis of brain dysfunction and skeletal dysplasia induced by NANS deficiency is worthwhile, not only because of the goal of elaborating therapeutic approaches for NANS-deficient individuals but also to shed light on sialic acid metabolism with its implications for human health.

URLs. Exome Aggregation Consortium (ExAC) database (accessed January 2016), http://exac.broadinstitute.org/; Wellderly database at the Scripps Wellderly Genome Resource, Scripps Wellderly Study (La Jolla, California) (accessed January 2016), https://genomics.scripps.edu/browser/files/wellderly/vcf/; PolyPhen-2 software for mutation assessment, http://genetics.bwh.harvard.edu/pph2/; Provean software for mutation assessment, http://provean.jcvi.org/index.php; Ensembl database, http://www.ensembl.org/; Novoalign software, http://www.novocraft.com/; Gaslini Cell Repository and Biobank, http://dppm.gaslini.org/biobank/; Leenaards Foundation in Lausanne, http://www.leenaards.ch/; Treatable Intellectual Disability Endeavor in British Columbia: First Collaborative Area of Innovation, http://www.tidebc.org/; Rare Diseases Models and Mechanisms Network, http://www.rare-diseases-catalyst-network.ca/index.php; Genome Analysis Toolkit (http://www.broadinstitute.org/gatk/); Enzyme Commission (EC) database, http://enzyme.expasy.org/.

METHODS

Methods and any associated references are available in the online version of the paper.

Note: Any Supplementary Information and Source Data files are available in the online version of the paper.

ACKNOWLEDGMENTS

We thank M. Filocamo at the Gaslini Biobank (Genoa, Italy) for a fibroblast line for patient 1. We thank A. Reymond (CIG, FBM, Université de Lausanne) and his laboratory for lymphocyte immortalization. We thank C. Chiesa for Sanger sequencing and sample handling and shipment; S. de Boer for excellent technical assistance; B. Toh at the University of British Columbia for metabolic sample handling; X. Han for Sanger sequencing; B. Sayson for consenting and data management; M. Higginson for DNA extraction and sample handling; and A. Ghani for administrative assistance. We also thank R. Houben for skillfully preparing **Figure 4** and A. Bandi for all other figures. We are grateful to our clinical colleagues in Dolo, Genoa, Lausanne, Manchester, Paris, Reggio Emilia, Tokyo, Treviso, and Vancouver for patient management. A.S.-F. dedicates this paper to the memory of Paolo Durand who pointed out the relationship between sialic acid metabolism and IDD to him in 1980. Finally, we wish to thank the patients reported here as well as their parents for the enthusiasm they showed for our research efforts, for their patience, which was challenged by the studies lasting many years, and for their repeated donation of biological samples. They have been the source of continuous motivation for us.

This work has been supported by funding from the Leenaards Foundation in Lausanne, Switzerland; the Faculty of Biology and Medicine of the University of Lausanne; the BC Children's Hospital Foundation (Treatable Intellectual Disability Endeavour in British Columbia: First Collaborative Area of Innovation); Genome BC (grant SOF-195); the Rare Diseases Foundation; the Rare Diseases Models and Mechanisms Network; the Canadian Institutes of Health Research (grant 301221); and the Dutch Organization for Scientific Research, ZONMW (Medium Investment Grant 40-00506-98-9001 and VIDI Grant 91713359 to D.J.L.). The zebrafish studies were supported by funding to X.-Y.W. from the Canadian Rare Disease Models and Mechanisms Network, the Brain Canada Foundation, the Natural Sciences and Engineering Research Council of Canada (NSERC), and the Canada Foundation for Innovation (CFI). The informatics infrastructures were supported by Genome BC and Genome Canada (ABC4DE Project) as well as by the Vital-IT Project of the Swiss Institute of Bioinformatics (SIB; Lausanne, Switzerland). C.J.R. is funded by a Canadian Institutes of Health Research New Investigator Award. C.D.M.v.K. is a recipient of the Michael Smith Foundation for Health Research Scholar Award (Vancouver, Canada). E.G. is supported by a Marie Skłodowska-Curie fellowship (MSCA-IF-661491).

AUTHOR CONTRIBUTIONS

C.D.M.v.K., L.B., S. Unger, R.A.W., and A.S.-F. conceived the study and coordinated and supervised the different teams. A.S.-F., L.B., C.D.M.v.K., T.D., A.C., M.I.V.A., C.J.R., J.H., L.G., L.T., V.C., D.H., D.D., C.B., I.M., and S. Uchikawa recruited the patients, reviewed the clinical and radiographic features, and obtained biological

materials from patients. A.S.-F., S. Unger, and G.N. reviewed the radiographic data. J.R. performed the bone marrow studies. Andrea Rossi reviewed the cerebral imaging. K. Harshman, B.J.S., B.C.-X., S.B., B.R.-B., H.R., C.R., M.T.-G., W.W.W., and A.d.B. were responsible for exome sequencing, haplotype reconstruction, Sanger sequencing, database studies, and mRNA–cDNA studies. R.A.W., L.A.J.K., E.v.d.H., and U.F.E. performed the metabolomics studies. Antonio Rossi studied ManNAc incorporation in fibroblasts. T. Hennet performed the lectin binding studies. A.A., K. Huijben, F.Z., and D.J.L. performed the NANS enzyme assays. D.J.L., A.A., T. Heisse, and T.B. studied the incorporation of sialic acid precursors in lymphocytes and fibroblasts. E.G. and G.S.-F. obtained the NANS three-dimensional model and mapped the affected amino acid residues. X.-Y.W. and K.B.-A. generated and phenotyped the zebrafish model. C.D.M.v.K. and A.S.-F. prepared the manuscript with contributions from all co-authors. All co-authors edited and reviewed the final manuscript.

COMPETING FINANCIAL INTERESTS

The authors declare no competing financial interests.

1. Salvador-Carulla, L. *et al.* Intellectual developmental disorders: towards a new name, definition and framework for "mental retardation/intellectual disability" in ICD-11. *World Psychiatry* **10**, 175–180 (2011).
2. American Psychiatric Association. *Diagnostic and Statistical Manual of Mental Disorders* 5th edn (American Psychiatric Publishing, 2013).
3. de Ligt, J. *et al.* Diagnostic exome sequencing in persons with severe intellectual disability. *N. Engl. J. Med.* **367**, 1921–1929 (2012).
4. Gilissen, C. *et al.* Genome sequencing identifies major causes of severe intellectual disability. *Nature* **511**, 344–347 (2014).
5. van Karnebeek, C.D.M. & Stockler, S. Treatable inborn errors of metabolism causing intellectual disability: a systematic literature review. *Mol. Genet. Metab.* **105**, 368–381 (2012).
6. Bonafé, L. *et al.* Nosology and classification of genetic skeletal disorders: 2015 revision. *Am. J. Med. Genet.* **167**, 2869–2892 (2015).
7. Superti-Furga, A., Bonafé, L. & Rimoin, D.L. Molecular-pathogenetic classification of genetic disorders of the skeleton. *Am. J. Med. Genet.* **106**, 282–293 (2001).
8. Camera, G., Camera, A., Di Rocco, M. & Gatti, R. Sponastrime dysplasia: report on two siblings with metal retardation. *Pediatr. Radiol.* **23**, 611–614 (1993).
9. Geneviève, D. *et al.* Exclusion of the dymeclin and PAPSS2 genes in a novel form of spondyloepimetaphyseal dysplasia and mental retardation. *Eur. J. Hum. Genet.* **13**, 541–546 (2005).
10. Tarailo-Graovac, M. *et al.* Exome sequencing and the management of neurometabolic disorders. *N. Engl. J. Med.* (in the press).
11. Cotton, T.R., Joseph, D.D., Jiao, W. & Parker, E.J. Probing the determinants of phosphorylated sugar-substrate binding for human sialic acid synthase. *Biochim. Biophys. Acta* **1844**, 2257–2264 (2014).
12. Galuska, S.P. *et al.* Quantification of nucleotide-activated sialic acids by a combination of reduction and fluorescent labeling. *Anal. Chem.* **82**, 4591–4598 (2010).
13. Büll, C. *et al.* Sialic acid glycoengineering using an unnatural sialic acid for the detection of sialoglycan biosynthesis defects and on-cell synthesis of siglec ligands. *ACS Chem. Biol.* **10**, 2353–2363 (2015).
14. Riemersma, M. *et al.* Disease mutations in CMP–sialic acid transporter *SLC35A1* result in abnormal α-dystroglycan O-mannosylation, independent from sialic acid. *Hum. Mol. Genet.* **24**, 2241–2246 (2015).
15. Link, V., Shevchenko, A. & Heisenberg, C.P. Proteomics of early zebrafish embryos. *BMC Dev. Biol.* **6**, 1 (2006).
16. Eisen, J.S. & Smith, J.C. Controlling morpholino experiments: don't stop making antisense. *Development* **135**, 1735–1743 (2008).
17. Javidan, Y. & Schilling, T.F. Development of cartilage and bone. *Methods Cell Biol.* **76**, 415–436 (2004).
18. Wang, B. & Brand-Miller, J. The role and potential of sialic acid in human nutrition. *Eur. J. Clin. Nutr.* **57**, 1351–1369 (2003).
19. Simpson, M.A. *et al.* Infantile-onset symptomatic epilepsy syndrome caused by a homozygous loss-of-function mutation of GM3 synthase. *Nat. Genet.* **36**, 1225–1229 (2004).
20. Hu, H. *et al. ST3GAL3* mutations impair the development of higher cognitive functions. *Am. J. Hum. Genet.* **89**, 407–414 (2011).
21. Fragaki, K. *et al.* Refractory epilepsy and mitochondrial dysfunction due to GM3 synthase deficiency. *Eur. J. Hum. Genet.* **21**, 528–534 (2013).
22. Boccuto, L. *et al.* A mutation in a ganglioside biosynthetic enzyme, *ST3GAL5*, results in salt & pepper syndrome, a neurocutaneous disorder with altered glycolipid and glycoprotein glycosylation. *Hum. Mol. Genet.* **23**, 418–433 (2014).
23. Mohamed, M. *et al.* Intellectual disability and bleeding diathesis due to deficient CMP–sialic acid transport. *Neurology* **81**, 681–687 (2013).
24. Roughley, P.J., White, R.J. & Santer, V. Comparison of proteoglycans extracted from high and low weight–bearing human articular cartilage, with particular reference to sialic acid content. *J. Biol. Chem.* **256**, 12699–12704 (1981).
25. Vincent, K. & Durrant, M.C. A structural and functional model for human bone sialoprotein. *J. Mol. Graph. Model.* **39**, 108–117 (2013).
26. Sodek, J., Ganss, B. & McKee, M.D. Osteopontin. *Crit. Rev. Oral Biol. Med.* **11**, 279–303 (2000).
27. Wang, B. Sialic acid is an essential nutrient for brain development and cognition. *Annu. Rev. Nutr.* **29**, 177–222 (2009).
28. Wang, B. Molecular mechanism underlying sialic acid as an essential nutrient for brain development and cognition. *Adv. Nutr.* **3**, 465S–472S (2012).
29. Sprenger, N. & Duncan, P.I. Sialic acid utilization. *Adv. Nutr.* **3**, 392S–397S (2012).
30. Salama, I. *et al.* No overall hyposialylation in hereditary inclusion body myopathy myoblasts carrying the homozygous M712T *GNE* mutation. *Biochem. Biophys. Res. Commun.* **328**, 221–226 (2005).
31. Malicdan, M.C., Noguchi, S., Hayashi, Y.K., Nonaka, I. & Nishino, I. Prophylactic treatment with sialic acid metabolites precludes the development of the myopathic phenotype in the DMRV-hIBM mouse model. *Nat. Med.* **15**, 690–695 (2009).
32. Oetke, C. *et al.* Evidence for efficient uptake and incorporation of sialic acid by eukaryotic cells. *Eur. J. Biochem* **268**, 4553–4561 (2001).
33. Nöhle, U. & Schauer, R. Uptake, metabolism and excretion of orally and intravenously administered, ^{14}C- and ^{3}H-labeled *N*-acetylneuraminic acid mixture in the mouse and rat. *Hoppe-Seyler's Z. Physiol. Chem.* **362**, 1495–1506 (1981).
34. Tangvoranuntakul, P. *et al.* Human uptake and incorporation of an immunogenic nonhuman dietary sialic acid. *Proc. Natl. Acad. Sci. USA* **100**, 12045–12050 (2003).
35. Samraj, A.N. *et al.* A red meat–derived glycan promotes inflammation and cancer progression. *Proc. Natl. Acad. Sci. USA* **112**, 542–547 (2015).
36. Bode, L. Human milk oligosaccharides: every baby needs a sugar mama. *Glycobiology* **22**, 1147–1162 (2012).
37. Fuhrer, A. *et al.* Milk sialyllactose influences colitis in mice through selective intestinal bacterial colonization. *J. Exp. Med.* **207**, 2843–2854 (2010).
38. Röhrig, C.H., Choi, S.S. & Baldwin, N. The nutritional role of free sialic acid, a human milk monosaccharide, and its application as a functional food ingredient. *Crit. Rev. Food Sci. Nutr.* doi:10.1080/10408398.2015.1040113 (2016).

ONLINE METHODS

Ethics. The studies were approved by the ethics boards of the following institutions: BC Children's and Women's Hospital, University of British Columbia (12-00067) and the Ethics Board of the Lausanne University Hospital. Research was performed according to the countries' ethics code of conduct. Parents or guardians provided written informed consent for the biochemical and genetic analysis and the publication of photographs and clinical data.

Identification of mutations in *NANS*. For patients 1–4, fragmented genomic DNA was purified with AMPure XP beads, and its quality was assessed with an Agilent Bioanalyzer. Preparation of the exome-enriched, barcoded sequencing libraries was performed using the SureSelect Human All Exon v4 kit (Agilent Technologies). The final libraries were quantified with a Qubit Fluorometer (Life Technologies), and the correct size distribution was validated on an Agilent Bioanalyzer. Libraries were then sequenced on a HiSeq 2000 machine (Illumina), generating 100-bp paired-end reads. Raw reads were aligned onto the hg19 reference genome using Novoalign software. Data cleanup and variant calling were performed according to GATK Best-Practices recommendations[39]. Variant filtering was performed with ANNOVAR[40] and with in-house Perl and Bash scripts, available upon request. For patient 9, who was genotyped in the Vancouver laboratory, similar procedures were used. To investigate the presence of a possible ancestral haplotype carrying the *NANS* indel in patients 1–4, we extracted all SNP alleles that were present in the region surrounding *NANS* and that were listed in the dbSNP database. Local genotypes were then scored, and likely haplotypes were constructed. In patients 5–8, all individual exons of *NANS* were amplified from genomic DNA (primer sequences available upon request) and sequenced directly in both directions using the Sanger method. For patient 9, exome sequencing was performed as part of the TIDEX gene discovery project using the Agilent SureSelect kit and an Illumina HiSeq 2000 instrument. The sequencing reads were aligned to human reference genome version hg19 (35× coverage), and rare variants were identified and assessed for their potential to disrupt protein function. In total, we identified 19 candidate genes affected by two rare heterozygous variants. Of these, *NANS* stood out as the most interesting functional candidate because of the preexisting next-generation metabolomics data. Sanger sequencing in the patient and his parents confirmed the mutations and their segregation with disease.

Construction of a three-dimensional protein model for NANS and mapping of the predicted mutations. A molecular model for dimeric full-length human NANS protein was generated with I-TASSER[41], using as templates the *N. meningitidis* homolog[42] and the human AFPL domain[43] structures. The model illustrations were generated with the PyMol Molecular Graphics System, version 1.7.4 (Schrödinger).

mRNA studies. Lymphoblastoid cell lines were cultured in suspension under 5% CO_2 in T25 flasks with RPMI-1640 medium supplemented with GlutaMAX-I (Gibco) containing 10% FBS (Gibco, 10270-106) and 1% penicillin-streptomycin (Gibco), whereas fibroblasts were cultured in DMEM (1×) with 1 g/L D-glucose L-glutamine (Gibco), supplemented with 10% FBS and 1% penicillin-streptomycin. To test for NMD, treatment with cycloheximide (Sigma-Aldrich) was performed in parallel with controls by incubating 10 million cells for 4 h in the presence of medium supplemented with 28 µg/ml of this chemical, according to published protocols[44]. Total RNA was isolated from both cycloheximide-treated and untreated fibroblast and lymphoblast cultures using the Direct-zol RNA MiniPrep kit (Zymo Research) according to the manufacturer's instructions. cDNA was prepared following the retrotranscription of 500 ng of RNA, using the PrimerScript RT–PCR kit (Clontech) and random hexamers; 10 ng of the produced cDNA was then used as template for downstream experiments. A specific primer pair spanning the exon–exon junctions for exons 1 and 2 and exons 5 and 6 (for sequences, see **Supplementary Table 5**) was designed to amplify the regions of the *NANS* cDNA containing all mutations studied. RT–PCR was performed in triplicate in a final reaction volume of 20 µl containing 5× Green GoTaq reaction buffer (Promega), 100 µM dNTP mix, 200 nM of each primer, and 0.1 U of GoTaq G2 DNA Polymerase (Promega). Reactions were incubated at 94 °C for 1 min followed by 35 cycles at 93 °C for 20 s, 64.1 °C for 30 s, and 72 °C for 1 min. The obtained products were resolved by capillary electrophoresis with the eGene HDA-GT12 Multi-Channel Genetic Analyzer, quantified, and finally ligated into the pCRII-TOPO TA vector (Invitrogen). Ligation mixes were used to transform chemically competent TOP-10 *Escherichia coli* (Invitrogen), and individual clones (at least 30 clones per electrophoresed sample) were sequenced by direct Sanger sequencing using BigDye terminator v1.1 (Applied Biosystems) with insert-specific primers. Sequencing data were analyzed using CLC Bio software (Qiagen) and compared with the corresponding human reference sequence (build hg19).

Next-generation metabolomics analysis. High-resolution untargeted metabolomics analysis of body fluids was performed using UHPLC–QTOF mass spectrometry. CSF and heparinized plasma samples were deproteinated in methanol:ethanol solution (50:50; 100 µl of each sample plus 400 µl of methanol:ethanol solution). Samples were analyzed in duplicate. A 2-µl sample was applied to an Acquity HSS T3 reverse-phase column (100 × 2.1 mm; 100 Å, 1.8 µm), and an Agilent 6540 UHD accurate mass UHPLC–QTOF mass spectrometer with acquisition in positive and negative modes was used. The buffers in positive mode consisted of buffer A (0.1 formic acid in water) and buffer B (0.1 formic acid in water:methanol solution (1:99)); in negative mode, the buffers consisted of buffer A (10 mM acetic acid) and buffer B (10 mM acetic acid in water:methanol solution (1:99)). After analysis and XCMS alignment, bioinformatics software developed in house showed the features (exact *m*/*z*, retention time, and intensity) deriving from metabolites that were significantly different in intensity in the patient sample as compared to age- and sex-matched controls. The Human Metabolome Database 3.0 was used to putatively annotate significantly different features[45]. This technique, also referred to as 'next-generation metabolic screening', was clinically validated using body fluids from patients for 25 known inborn errors of metabolism and introduced in the Nijmegen patient care research setting.

Proton (^{1}H) NMR spectroscopy of body fluids, fibroblast homogenates, and model compounds of N-acetylated sugars was performed on a 500-MHz NMR spectrometer with minor modifications[46]. The NMR spectrum for fibroblasts was recorded on a homogenate obtained after sonicating 7.5×10^6 cells in ^2H_2O (D_2O). The homogenate was deproteinated over a 10 kDa filter and trimethylsilyl-2,2,3,3-tetradeutero propionic (TSP) acid was used as a chemical shift reagent in the NMR spectrum. The model compounds ManNAc, *N*-acetylgalactosamine, and *N*-acetylglucosamine were purchased from Sigma Chemicals, and ManNAc-6-phosphate was purchased from Carbosynth (disodium salt).

Lectin staining on cultured fibroblasts. Fibroblasts were cultured for 48 h in DMEM supplemented with 10% FCS and 0, 1, or 10 mM ManNAc. After incubation, fibroblasts were trypsinized, washed twice in Hank's buffered saline solution (HBSS) containing 1% FCS, and resuspended at 1×10^6 cells/ml. Aliquots of 1×10^5 cells (in 100 µl) were incubated with 1 mM FITC-labeled *S. nigra* lectin (Vector Labs) in HBSS for 20 min on ice, washed twice in HBSS containing 1% FCS, and analyzed by flow cytometry using a FACSCanto II cytometer (BD Biosciences).

***N*-acetylmannosamine incorporation in fibroblast culture.** Skin fibroblasts were cultured and expanded in DMEM supplemented with 10% FCS at 37 °C in 5% CO_2 and were then cultured for 24 h in the absence of FCS. For the incorporation experiment, mycoplasma-negative cells were incubated in DMEM, without serum and antibiotics, with or without 10 mM ManNAc, at 37 °C in 5% CO_2 for 48 h. After incubation, the medium was removed, and cells were harvested in PBS and collected by low-speed centrifugation. The cell pellet was sonicated in buffer containing 20 mM Tris-HCl, pH 8.0, 5 mM EDTA, 150 mM NaCl, 1 µg aprotinin, and 1 mM PMSF, and the lysate was ultracentrifuged at 30,000*g* for 1 h at 4 °C to pellet the membrane fraction. In the clear supernatant, protein content was determined with the BCA protein assay (Pierce), and aliquots of the supernatant were ultrafiltered with an Amicon Ultra-0.5 Centrifugal Filter Unit with a cutoff of 3 kDa to separate sialic acid from soluble protein. The dried filtrate was used for sialic acid analysis. The CMP–sialic acid content was discriminated from free sialic acid by reduction: labeling with the fluorophore 1,2-diamino-4,5-methylenedioxybenzene (DMB) requires free keto as

well as carboxyl groups on the sialic acid molecule, and reduction of the keto group before the labeling process precludes the labeling of non-activated sialic acid[12]. Each lyophilized sample was split in two aliquots. To reduce free, non-activated monosaccharides, the dried samples were dissolved in 0.2 M sodium borate buffer, pH 8.0, containing 0.2 M sodium borohydride, incubated at 0 °C overnight, and dried in a SpeedVac concentrator. For fluorescent labeling of sialic acid, samples were hydrolyzed in 0.2 N trifluoroacetic acid (TFA) for 4 h at 80 °C, dried, redissolved twice in methanol, and dried again. To label sialic acids with DMB, hydrolysates were dissolved in 80 µl of 0.64 mg/ml DMB in 500 mM 2-mercaptoethanol, 9 mM sodium hydrosulfite, and 20 mM TFA and incubated for 2 h at 56 °C. Reactions were stopped by adding 10 µl of 0.2 M NaOH. The derivatized sialic acids were quantified by HPLC on a binary pump system (1525 Binary HPLC Pump, Waters) coupled to a fluorescence detector (2475 Multy λ Fluorescence Detector, Waters) set at an excitation wavelength of 372 nm and an emission wavelength of 456 nm. Chromatography was carried out at room temperature with a LichroCART 250-4 Superspher 100 RP18 (250 × 4 mm) column (Merck) and LiChrospher 100 RP18 (25 × 4 mm) (Merck) as a pre-column. Mobile phases were methanol:acetonitrile:water:TFA (4:4:92:0.1) and methanol:acetonitrile:water:TFA (45:45:10:0.1), and the flow rate was 0.3 ml/min[12].

Measurement of the *N*-acetylneuraminic acid content in fibroblasts. Fibroblasts (~2.5 million cells) in 250 µl of 50 mM Tris-HCl, pH 7.5, were sonicated on ice (3 × 8 s) and then centrifuged (10,000*g* for 10 min at 4 °C). To 100 µl of the supernatant (lysate) was added [3-^{13}C]NeuNAc (±23 µM) as an internal standard, and the solution was applied to a 30-kDa filter cup (Amicon Ultra) with 10 µl of 2% formic acid in the collection tube for deproteination. After centrifugation at 13,000*g* for 30 min at 4 °C, the flow-through was used for quantification of NeuNAc by mass spectrometry according to published methods[47,48]. Assays were performed in duplicate, and NeuNAc levels were normalized to protein levels in the lysates.

Determination on NANS activity in fibroblast cultures. Skin fibroblasts were obtained from affected individuals and healthy controls and cultured at 37 °C under 5% CO_2 in culture medium E199, supplemented with 10% FCS and 1% penicillin-streptomycin. All cultures were tested for mycoplasma infection before growth in culture. We developed an assay for NANS activity as follows: fibroblasts (~7.5 million cells) in 300 µl of 50 mM Tris-HCl, pH 7.5, were sonicated on ice (3 × 8 s) and then centrifuged (10,000*g* for 10 min at 4 °C). The supernatant (lysate) was used for the determination of protein concentration (BCA assay) and for enzyme activity assays. Incubation of ManNAc-6-phosphate disodium salt (Carbosynth; 2 mM) and 20 µl of lysate was carried out at 37 °C in duplicate in a total reaction volume of 100 µl. The reaction buffer consisted of 50 mM Tris-HCl, pH 7.5, 3 mM PEP (Roche), and 1 mM $MgCl_2$. Control incubations without ManNAc-6-phosphate were subtracted as a blank from the incubations. The reactions were allowed to proceed for 2.5, 5, and 24 h and then stopped by freezing (–20 °C). Samples (100 µl) were deproteinated by the addition of 50 µl of [3-^{13}C]NeuNAc (±23 µM) as an internal standard and centrifuged at 13,000*g* for 30 min at 4 °C on a 30-kDa filter cup (Amicon Ultra); the flow-through was collected in 10 µl of 2% formic acid. NeuNAc levels were quantified by mass spectrometry as described[47,48] and normalized for protein level in the lysates.

Metabolic labeling of sialic acids and glycoproteins in fibroblast cultures. Skin-derived fibroblasts were cultured in M199 medium (PAN biotech) supplemented with 10% FBS (PAA), non-essential amino acids (NEAA; Gibco), and 100 U/ml penicillin-streptomycin (Gibco) and tested for mycoplasma contamination. Eighty percent confluent cells were further grown for 5 d in medium containing 15 µM Ac5NeuNAc, Ac4ManNPoc, or Ac5NeuNPoc. Cells were collected in PBS by scraping and lysed in 150 mM NaCl, 50 mM Tris-HCl, pH 7.5, 5 mM EDTA, 0.1% SDS, 1% Triton X-100, and 1× Complete protease inhibitor cocktail (Roche). To biotinylate propargyloxycarbonyl-containing glycoproteins, cell lysates were resolved on 10% SDS gels, blotted onto PVDF membrane. Unoccupied membrane sites were blocked with 5% dry milk in PBS, and the membrane was incubated with 500 µM $CuSO_4$, 250 µM l-histidine, 100 µM azide-PEG3-biotin, and 500 µM sodium ascorbate in PBS for 1 h at 37 °C. Biotinylated sialoglycoproteins were visualized by incubation with horseradish peroxidase (HRP)-conjugated streptavidin (GE Healthcare), followed by signal development with SuperSignal West Femto Maximum-Sensitivity Substrate (Thermo Fisher Scientific). As a loading control, immunostaining was performed with antibody to GAPDH (Abcam, ab8245) on the same membranes. On the basis of this protocol, we found that NeuNPoc at 15 µM concentration would readily label cellular sialoglycans after 5 d of incubation. For ManNPoc at the same concentration of 15 µM, longer incubation times were required to obtain strong labeling of glycoconjugates in fibroblasts from healthy donors (**Fig. 5**).

Determination of glycosylation of plasma proteins. Analysis of plasma transferrin N-glycosylation was carried out by isoelectric focusing[49] as well as by nanochip QTOF mass spectrometry[50]. The mucin-type O-linked glycosylation of plasma apolipoprotein C-III was analyzed by isoelectric focusing[49].

Zebrafish studies. Zebrafish were maintained at 28.5 °C on a 10-h dark/14-h light cycle. Protocols for experimental procedures were approved by the Research Ethics Board of St. Michael's Hospital (Toronto) (protocol ACC660). To knock down gene expression, we used splicing-blocking MOs for *nansa* and *nansb* knockdown plus a standard control MO (for sequences, see **Supplementary Table 5**). The zebrafish *nansa* gene has six exons, with the translation start codon in exon 1 (ENSDART00000067086; chromosome 1). We designed a splicing-blocking MO nansa-e3i3 that could block the splicing donor of exon 3, resulting in intron 3 retention and a truncated protein in translation (data not shown). *nansb* also has six exons, with the translation start codon in exon 1 (ENSDART00000169540; chromosome 25), and we designed an MO nansb-e1i1 to block the splicing donor site of exon 1 of *nansb*, resulting in intron 1 retention and a truncated Nansb protein (data not shown). MOs were synthesized by Gene Tools (for sequences, see **Supplementary Table 5**) and microinjected individually or in combination into zebrafish embryos at the one-cell stage. We injected embryos individually with nansa-e3i3 (4 ng/nl) and nansb-e1i1 (4 ng/nl) MOs, and also coinjected embryos with nansa-e3i3 (4 ng/nl) and nansb-e1i1 (4 ng/nl). Each injection was repeated at least three times. Knockdown of *nansa* and *nansb* was assessed by RT–PCR to confirm splicing defect and retention of the intron (data not shown). For control MO, embryos were injected at the one-cell stage with 4 ng/nl. At least 30 embryos were injected per condition and included in the analysis. At 24 h.p.f., embryos were manually dechorionated. Total RNA was extracted from embryos at 48 h.p.f. using TRIzol reagent (Invitrogen). The RNA concentration of each sample was determined using a NanoDrop ND-1000 spectrophotometer (NanoDrop Technologies). RNA integrity was verified by 1% agarose gel electrophoresis. The RNA template was converted into cDNA using Superscript II reverse transcriptase (Invitrogen) and used to amplify a *nansa*-specific cDNA (for primer sequences, see **Supplementary Table 5**).

To visualize the cartilaginous structures, Alcian blue (Sigma) was dissolved in 70% ethanol and 1% hydrochloric acid. Zebrafish embryos (6 d.p.f.) were fixed in 4% paraformaldehyde overnight at 4 °C and maintained in 100% methanol at –20 °C until processing. The embryos were washed with PBS containing 0.1% Tween-20 (PBST). The embryos were bleached in 30% hydrogen peroxide for 2 h, washed with PBST, and transferred into Alcian blue solution. Embryos were stained overnight at room temperature. The embryos were rinsed four times with acidified ethanol (HCl-EtOH); 5% hydrochloric acid and 70% ethanol. Embryos were rinsed for 20 min in HCl-EtOH and rehydrated by washing 10 min in an HCl-EtOH/H_2Od series (75%, 25%, 50%, 50%, 25%, and 75%) and 100% H_2Od. Embryos were stored in 1 ml of glycerol-KOH.

39. Van der Auwera, G.A. *et al.* From FastQ data to high confidence variant calls: the Genome Analysis Toolkit best practices pipeline. *Curr. Protoc. Bioinformatics* **43**, 1–33 (2013).
40. Wang, K., Li, M. & Hakonarson, H. ANNOVAR: functional annotation of genetic variants from high-throughput sequencing data. *Nucleic Acids Res.* **38**, e164 (2010).
41. Yang, J. *et al.* The I-TASSER Suite: protein structure and function prediction. *Nat. Methods* **12**, 7–8 (2015).
42. Gunawan, J. *et al.* Structural and mechanistic analysis of sialic acid synthase NeuB from *Neisseria meningitidis* in complex with Mn^{2+}, phosphoenolpyruvate, and *N*-acetylmannosaminitol. *J. Biol. Chem.* **280**, 3555–3563 (2005).
43. Hamada, T. *et al.* Solution structure of the antifreeze-like domain of human sialic acid synthase. *Protein Sci.* **15**, 1010–1016 (2006).

doi:10.1038/ng.3578

44. Rajavel, K.S. & Neufeld, E.F. Nonsense-mediated decay of human *HEXA* mRNA. *Mol. Cell. Biol.* **21**, 5512–5519 (2001).
45. Wishart, D.S. *et al.* HMDB 3.0—the Human Metabolome Database in 2013. *Nucleic Acids Res.* **41**, D801–D807 (2013).
46. Engelke, U.F. *et al.* NMR spectroscopic studies on the late onset form of 3-methylglutaconic aciduria type I and other defects in leucine metabolism. *NMR Biomed.* **19**, 271–278 (2006).
47. Valianpour, F., Abeling, N.G., Duran, M., Huijmans, J.G. & Kulik, W. Quantification of free sialic acid in urine by HPLC–electrospray tandem mass spectrometry: a tool for the diagnosis of sialic acid storage disease. *Clin. Chem.* **50**, 403–409 (2004).
48. van der Ham, M. *et al.* Liquid chromatography–tandem mass spectrometry assay for the quantification of free and total sialic acid in human cerebrospinal fluid. *J. Chromatogr. B Analyt. Technol. Biomed. Life Sci.* **878**, 1098–1102 (2010).
49. Jansen, J.C. *et al.* CCDC115 deficiency causes a disorder of Golgi homeostasis with abnormal protein glycosylation. *Am. J. Hum. Genet.* **98**, 310–321 (2016).
50. van Scherpenzeel, M., Steenbergen, G., Morava, E., Wevers, R.A. & Lefeber, D.J. High-resolution mass spectrometry glycoprofiling of intact transferrin for diagnosis and subtype identification in the congenital disorders of glycosylation. *Transl. Res.* **166**, 639–649 (2015).